

https://dspace.org/

ThreeDimensional Numerical Analysis on the Behaviour of GeocellReinforced Retaining Structures

S Shiwani; A.K Choudhary; Ganesh Rathod

https://hdl.handle.net/10539/40503
SCOPUS

Downloaded from a DSpace repository. https://dspace.org/

Transportation Infrastructure Geotechnology (2024) 11:1963–1988
https://doi.org/10.1007/s40515-023-00360-9

TECHNICAL PAPER

Three-Dimensional Numerical Analysis on the Behaviour of Geocell-Reinforced Retaining Structures

Shiwani[1] · Awdhesh Kumar Choudhary[2] · Ganesh W. Rathod[3]

Accepted: 26 November 2023 / Published online: 11 December 2023
© The Author(s), under exclusive licence to Springer Science+Business Media, LLC, part of Springer Nature 2023

Abstract

The demand for geocell-reinforced retaining walls has increased due to the rising requirements of infrastructural development and constraints in land use. The cumbersome geometry of geocell poses challenges when it comes to numerical modelling. In this study, the geocell-reinforced retaining walls have been modelled using 3D finite element method to investigate the behaviour of the retaining wall by introducing multiple layers of actual honeycomb-shaped geocell mattresses. The result indicates that the provision of reinforcement significantly increases the stability of the retaining wall system. The lateral deformation in the retaining wall increases with an increase in both surcharge load and the wall's facing angle. The factor of safety was found to decrease by nearly 1.75 times with an increase in the wall's facing angle from 50 to 80°. With an increase in the height of the geocell mattress from 125 to 250 mm, a significant reduction in lateral displacement was observed. However, further increase in the height of the geocell mattress shows marginal effect on the performance of the composite wall system. Besides, the proposed model shows encouraging agreement with the experimental results indicating that the present model can be used to study the behaviour geocell reinforcement retaining wall system.

Keywords Retaining wall · Geocell reinforcement · Numerical model · Soil

✉ Awdhesh Kumar Choudhary
awdhesh.ce@nitjsr.ac.in

Shiwani
2021pgcege11@nitjsr.ac.in

Ganesh W. Rathod
ganesh.rathod@wits.ac.za

[1] Department of Civil Engineering, National Institute of Technology Jamshedpur, Jamshedpur, Jharkhand 831014, India

[2] Department of Civil Engineering, National Institute of Technology Jamshedpur, Jamshedpur, Jharkhand 831014, India

[3] School of Civil and Environmental Engineering, University of the Witwatersrand, Johannesburg, 1 Jan Smuts Ave, Braamfontein, Johannesburg 2017, South Africa

List of Symbols

μ	Poisson's ratio
ψ	Dilation angle (°)
ϕ	Friction angle (°)
α	Wall's facing angle/sloping angle (°)
E	Young's modulus (MPa)
C	Cohesion (kPa)
l_e	Global meshing parameter
U_x	Horizontal displacement (m)
H	Height of the retaining wall (m)
h	Geocell height (m)
q	Surcharge (kPa)
K	Stiffness of geocell (kN/m)
GRRW	Geocell-reinforced retaining wall
URW	Unreinforced retaining wall
FOS	Factor of safety

1 Introduction

A retaining structure is generally designed to retain the earth behind it, by preventing the backfill from collapsing, slipping, and eroding. In the past few decades, due to an increase in infrastructural development demands and land use limitations, geosynthetic reinforcements have been widely used for the construction of steep slopes. Different products like geotextile and geogrid which are planar in nature used to increase the stability of the retaining wall (Zornberg et al., 1998; Bathurst et al., 2001; Rowe & Skinner, 2001; Benjamim et al., 2007). However, an advanced way to reinforce soil is by using a 3D geosynthetic product called geocell reinforcement. Geocell is the only 3D geosynthetic product that is formed by interconnecting polymeric sheets such as high-density polyethylene in a cellular fashion which provides all-around confinement to the soil mass. This type of confinement greatly improves the shear strength of the granular soil leading to an enhanced bearing capacity of the system. Several investigators used 3D cells that were prepared in the laboratory using materials like geotextile, geogrid, papers, and bamboo (Bush et al., 1990; Krishnaswamy et al., 2000; Dash et al., 2001; Dash et al., 2003; Chen & Chiu, 2008; Latha & Somwanshi, 2009; Hegde & Sitharam, 2014; Hegde & Sitharam, 2015; Hegde & Sitharam, 2017; Dash & Choudhary., 2018; Choudhary et al., 2019; Arvin et al., 2022). It was reported that the performance of soil beds can be greatly enhanced by providing a layer of geocell reinforcement within the course of the soil mass.

In regard to the geocell-reinforced retaining wall, that is commonly employed to prevent the lateral movement of backfill material effectively. A number of studies on the reinforced retaining wall/slope were reported in the past. A 2D analysis on the behaviour of embankment, reinforced with geocell was performed by Latha and Rajagopal (2007). In the above analysis, the layer of geocell was considered as a soil layer that possessed increased cohesive strength and stiffness due to the influence

of confinement. Further, Mehdipour et al. (2013) numerically explored the behaviour of geocell-reinforced slopes using the strength reduction method. The geocell layer was modelled using beam elements in FLAC^{2D} (Fast Lagrangian Analysis of Continua), which are capable of carrying both bending and membrane stresses. To examine the influence of the geocells as primary material in retaining structures under the surcharge load, a series of model tests on the geocell-reinforced retaining walls (GRRW) system were performed by Chen and Chiu (2008). It was reported that the facing type walls show more displacement and settlement than the gravity type due to their lighter weight. By validating the result of the model test, Chen et al. (2013) analysed four different layouts of the geocell-reinforced retaining walls using the finite difference method (FLAC). The findings indicated that extending the geocell layer at specific depths from top to bottom could be an effective construction technique in terms of minimising wall movement and backfill settlement. The geocell layers were simulated with the help of the equivalent approach method in the above study.

As per the assessment of the literature, it seems that geocell is modelled either as the equivalent composite approach (Hegde & Sitharam, 2014; Latha et al., 2009; Song et al., 2017; Halder & Chakraborty, 2020) or as a square box shape (Song et al., 2018). In the equivalent composite approach, the geocell–soil composite is assumed as a soil layer with better strength and stiffness. However, modelling geocell as a soil layer appears to be unrealistic. Secondly, when a geocell is designed as a square box, it is observed that stresses have a tendency to accumulate primarily at the corner edges of the box. This accumulation, in turn, can result in inaccuracies. On the other hand, the honeycomb structure of the geocell effectively mitigates this issue by distributing the stresses uniformly along the entire periphery. As a result, this uniform distribution ensures a more precise and accurate outcome (Hegde & Sitharam, 2014). In order to get an accurate performance of the system, it is essential to study the behaviour of the geocell-reinforced retaining wall considering the actual curvature of the expanded geocell. In view of this, the behaviour of the geocell-reinforced wall considering the actual curvature of the expanded geocell has been analysed using the three-dimensional finite element method (PLAXIS^{3D}). Further, the influence of several other parameters such as the effect of the wall's facing angle, surcharge, axial stiffness of the geocell, height of the geocell, friction, and dilation angle of the soil mass has also been investigated on the overall behaviour of the geocell-reinforced retaining wall system.

2 Methodology

The finite element program PLAXIS^{3D} is used to develop and analyse the model of unreinforced and reinforced retaining wall system. PLAXIS^{3D} is a geotechnical engineering–based finite element program designed primarily for deformation, stability, and flow analysis in engineering applications. The program employs a user-friendly graphical user interface that allows users to easily create a geometric model. For the unreinforced retaining wall, the prepared model has a dimension of 20 m × 10 m × 6 m which has been shown in Fig. 1. The dimension of the geocell-reinforced retaining

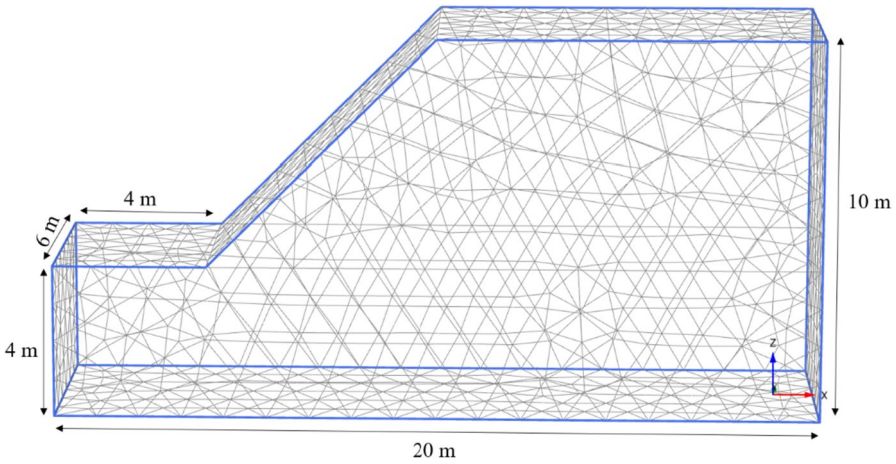


Fig. 1 Numerical model prepared for unreinforced retaining wall for validation

wall is 1.2 m × 0.345 m × 1 m as presented in Fig. 2a. The honeycomb structure of the geocell is adopted in this study which has been drawn in AutoCAD 2020 with the help of spline shown in Fig. 2b. Thereafter, it is extracted from AutoCAD with extension (.dxf) through the "import" tab available in the structure section of PLAXIS^{3D}. The extracted polycurves are extruded in the Z-direction with the required height of the geocell shown in Fig. 2c. Then, geocell mattresses are organised in eight layers by using their coordinates according to the facing angle of the wall, which has been illustrated in Fig. 2d, e, and f. Each layer has a different number of cells, shown in Fig. 2g. For soil–structure interaction, an interface is provided all around the geocell with a strength reduction factor equal to 0.67. The surface load is applied to the wall, which is available in the structure section. To simulate the behaviour of soil, the Mohr-Coulomb constitutive model also known as the linear elastic perfectly plastic model was used. There are five input parameters required by this type of model, viz., Young's modulus (E) and Poisson's ratio (μ) for soil elasticity, friction angle (ϕ) and cohesion (c) for soil plasticity, and the dilatancy angle (ψ). The properties of the soil used in this study are listed in Table 1. Geocell is a predefined structural element in PLAXIS which uses an elastic geogrid model. The properties of the geocell used in this study are listed in Table 2. When the geometric model is fully defined, in order to perform the finite calculations, it is divided into finite elements known as mesh. The generation of finite element mesh is fully automatic in PLAXIS^{3D}. The mesh generation process considers all the soil stratigraphy as well as all structural objects, loads, and boundary conditions. The boundary condition of the model is such that the bottom boundary is fixed against movement in all directions while the vertical boundary is allowed to move in a vertical direction and restricted in the horizontal direction. The basic soil elements in 3D finite element mesh are 10-node tetrahedral elements. Geocells are formed by 6-node triangular surface elements with 3 translational degrees of freedom (u_x, u_y, u_z) per node, and 12-node interface elements are used to simulate the behaviour of soil–structure interaction. The mesh generator requires a global meshing parameter (le), which represents the target

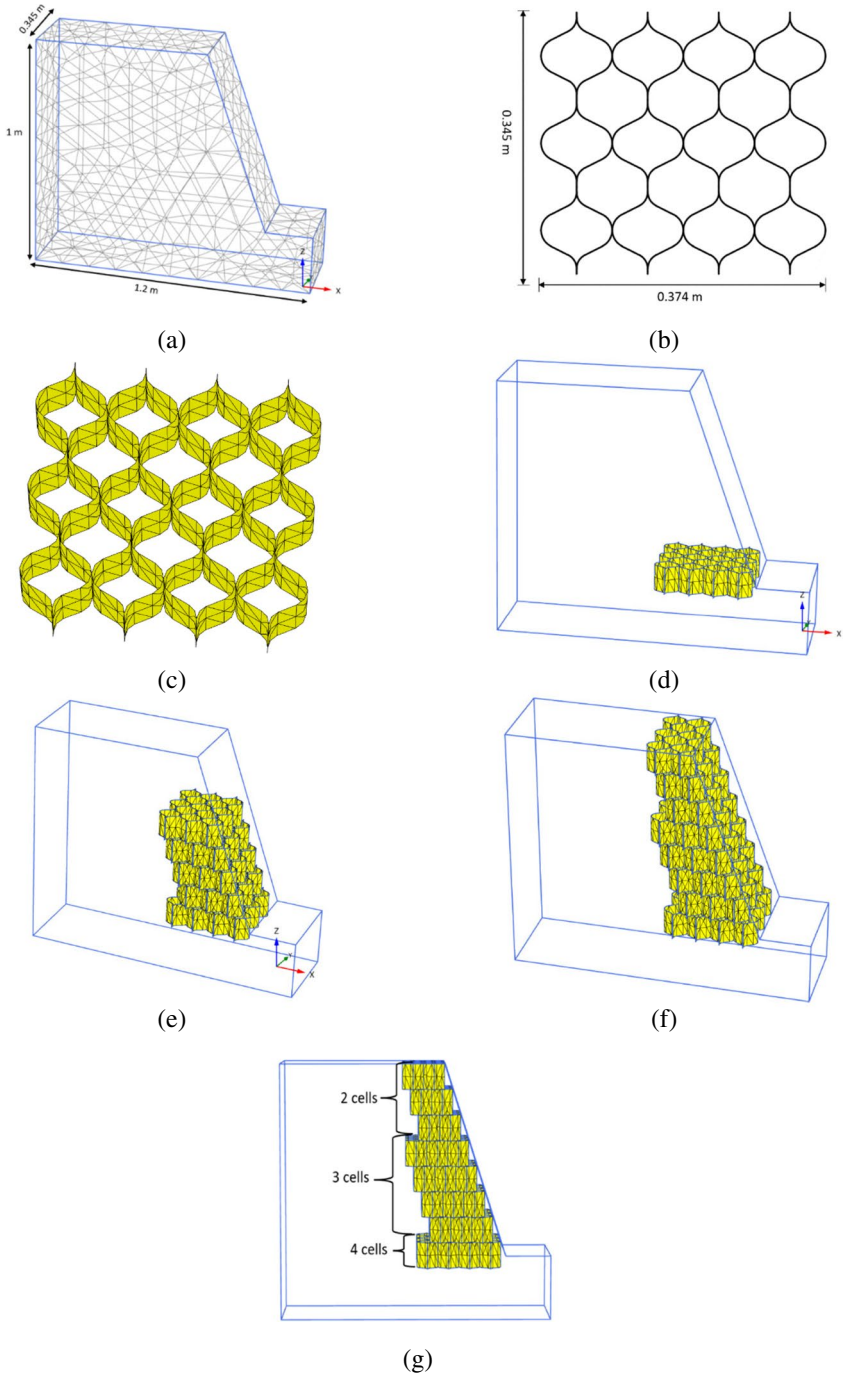


Fig. 2 Detailed geometry of the prepared model for geocell-reinforced retaining wall

Table 1 Properties of the sand used in the study

Soil parameter	Value
Young's modulus (MPa)	13.88
Unit Weight (kN/m^3)	15.3
Poisson's Ratio	0.33
Cohesion (kPa)	1
Friction angle (°)	35

Table 2 Properties of geocell used in the study

Material properties	Value
Tensile strength (kN/m)	17
Elastic modulus (kN/m)	492
Thickness (mm)	1.3

element dimension. This parameter is calculated from the outer geometry dimensions and the element distribution. There are basically five levels of element distribution; very coarse, coarse, medium, fine, and very fine. The mesh should be generated in such a way that it could validate the experimental results. It is advisable to avoid using very fine meshes as they can significantly increase computation time due to the increase in the number of elements especially for large-scale models. That is why, fine, medium, and coarse meshes are generated for walls having a facing angle equal to 70° to check the accuracy of the model. The generated mesh contains 58,124; 38,291; and 29,887 numbers of 10-noded elements with 132,898; 88,050; and 63,360 numbers of nodes for fine, medium, and coarse element distribution, respectively. Moreover, the fine mesh takes much higher calculation time while the medium mesh and coarse mesh take less calculation time. The influence of the mesh size (i.e., coarse, medium, and fine) on the facing displacement of the wall is presented in Fig. 3. It can be seen that the facing displacement increases with the increase in mesh size (i.e., from fine to coarse). It indicates that the fine mesh provides more resistance to lateral deformation. However, the coarse element distribution was found to be appropriate for simulating the behaviour of reinforced retaining walls as it is very close to experimental results. Therefore, even for a facing angle equal to 80°, a coarse mesh is generated in the model. Figure 4 shows the model walls having different facing angles of 70 and 80° generated using a coarse mesh for numerical validation with the experimental results.

3 Result and Discussion

3.1 Validation of the Numerical Model Through Existing Studies

Prior moving to the comprehensive numerical analysis, it is necessary to validate the proposed numerical model through existing studies to ascertain the correctness of the result. In view of this, the model of unreinforced retaining walls has been

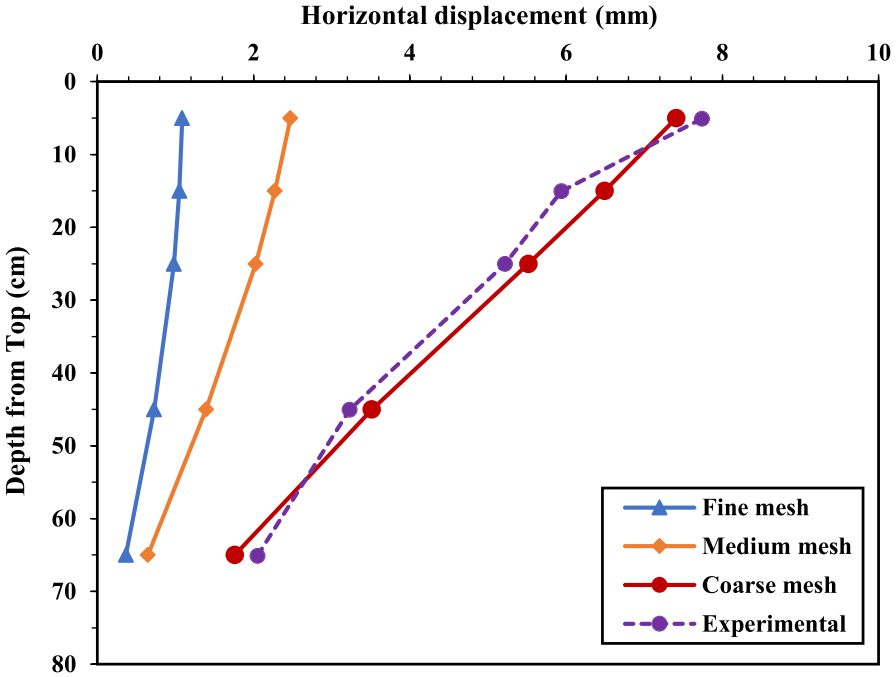


Fig. 3 Comparison of facing displacement for various meshes and experimental result

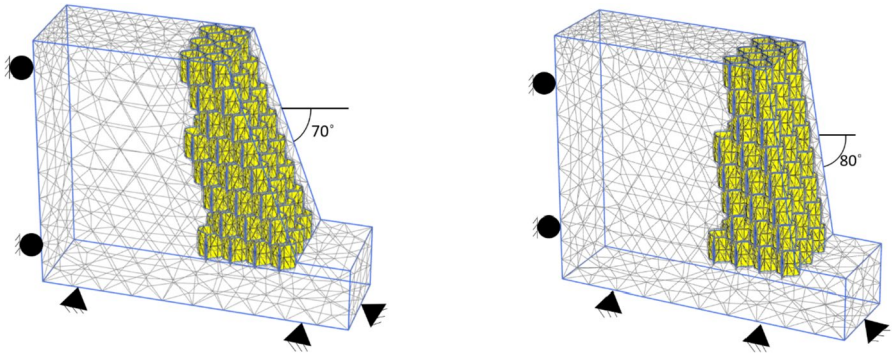


Fig. 4 Numerical model prepared for validation with boundary condition

validated from (Cheng et al., 2007). The factor of safety of the retaining wall is determined using the limit equilibrium method in 2D by keeping soil parameters (i.e., Young's modulus, Poisson's ratio, and unit weight) constant and varying the shear strength parameter of the soil (i.e., cohesion and friction angle). To analyse the unreinforced and reinforced retaining wall, the model needs to be prepared in 3D owing to the three-dimensional shape of the geocell. Moreover, the three-dimensional analysis is more authentic in being able to account for fixity and geometry

in the third dimension. This leads to enhanced accuracy as well as the understanding of the principle underlying the slope failure mechanism. Hence, in the present analysis, the model is prepared in 3D keeping the dimension the same as (Cheng et al., 2007), and the factor of safety has been determined using the strength reduction method. The obtained factor of safety and reported FOS is shown in Table 3, for comparison purposes. It is found that the obtained FOS is slightly greater than the previously reported study. This is because the shear strength mobilised in the case of 3D is more than that of 2D. Similar behaviour has been observed by (Griffiths & Marquez, 2007).

Further, the model of geocell-reinforced retaining wall used in this study is validated through the experimental results of Chen and Chiu (2008). The dimension of the proposed model is kept the same as considered (Chen & Chiu, 2008). The property of the soil and the geocell has also been adopted from the same. A typical model developed to simulate with existing study is presented in Fig. 4. Surcharge is applied on the top of the model wall and the horizontal displacement of the wall is determined. Figure 5 presents the comparison of numerical and experimental results. The validation between the experimental and numerical analysis is found to be in good agreement with a certain amount of error. Hence, it can be said that the current model developed in PLAXIS^{3D} is able to simulate the behaviour of a geocell-reinforced retaining wall system. In view of this, further detailed analyses have

Table 3 Comparison of factors of safety between the previously reported and present study

Case	C′(kPa)	ϕ (°)	FOS (LEM)	FOS (SRM)	FOS (present study)
1	2	5	0.25	0.25	0.27
2	2	15	0.5	0.51	0.53
3	2	25	0.74	0.77	0.79
4	2	35	1.01	1.07	1.09
5	2	45	1.35	1.42	1.47
6	5	5	0.41	0.43	0.44
7	5	15	0.7	0.73	0.75
8	5	25	0.98	1.03	1.04
9	5	35	1.28	1.34	1.36
10	5	45	1.65	1.68	1.76
11	10	5	0.65	0.69	0.69
12	10	15	0.98	1.04	1.05
13	10	25	1.3	1.36	1.38
14	10	35	1.63	1.69	1.73
15	10	45	2.04	2.05	2.17
16	20	5	1.06	1.2	1.2
17	20	15	1.48	1.59	1.58
18	20	25	1.85	1.95	1.97
19	20	35	2.24	2.28	2.38
20	20	45	2.69	2.67	2.87

been carried out to investigate the influence of several parameters on the overall behaviour of large-scale geocell-reinforced retaining wall systems, which has been presented and discussed in the following section.

3.2 Behaviour of the Unreinforced and Reinforced Retaining Wall

A retaining wall having a dimension of 6 m × 1 m × 4 m has been modelled with and without geocell reinforcement. The facing angle of the retaining wall has been taken at 50°. For geocell-reinforced retaining walls, the geocell mattresses are inserted in multiple layers. The geocell is provided with a cell dimension of 250 mm × 210 mm and a cell height of 250 mm. There are sixteen layers of geocell mattresses incorporated into it with varying numbers of cells in each layer. The complete geometry of the geocell-reinforced retaining wall is shown in Fig. 6. Figure 7 represents the facing displacement of the wall with and without the inclusion of the geocell reinforcement. It can be seen that the horizontal displacement is much larger for unreinforced retaining walls than for reinforced walls. The maximum displacement obtained for unreinforced and reinforced walls is 0.95 mm and 0.18 mm, respectively. The displacement decreases by nearly 81% with the inclusion of the geocell reinforcement. For both retaining walls, the maximum displacement occurs at 0.5625 H from the bottom of the wall. This can be clearly observed from the contour of the horizontal displacement of the wall. Figure 8a and b shows the contour of the horizontal displacement of the unreinforced retaining wall and geocell-reinforced

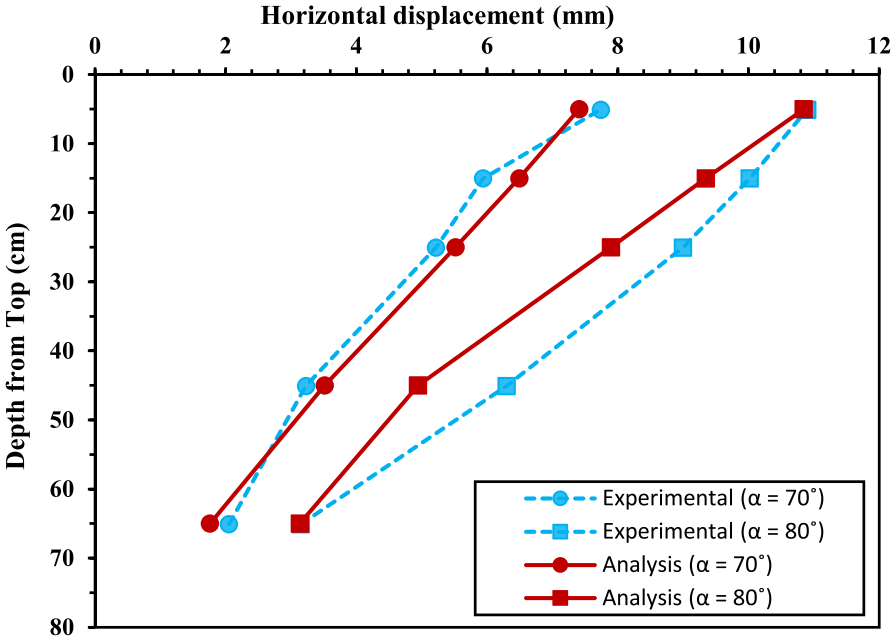


Fig. 5 Comparison of the experimental and numerical results at surcharge $q = 45$ kpa

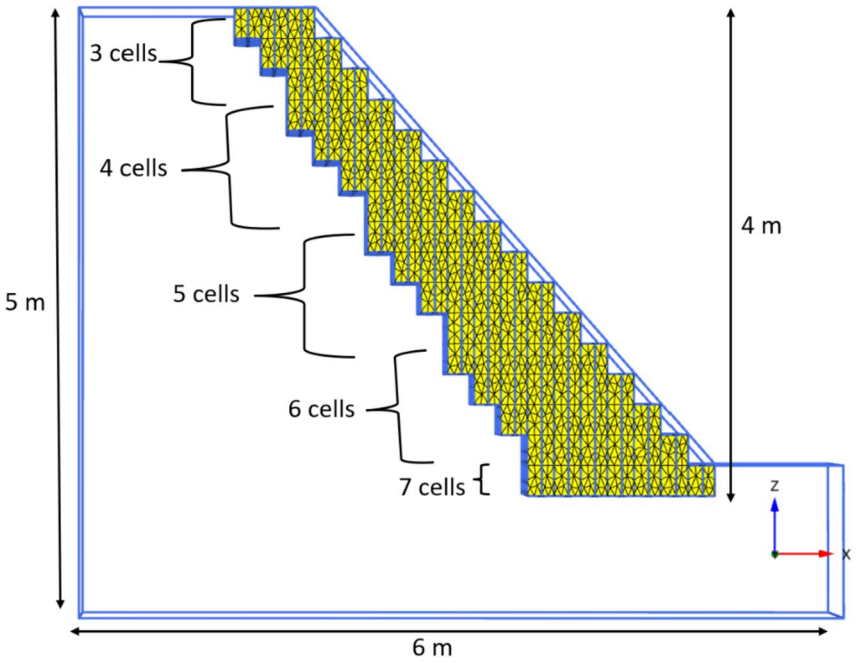


Fig. 6 Geometry of geocell-reinforced retaining wall at a sloping angle of 50°

wall, respectively. It can be inferred from these figures that the pattern of contour displacement is almost similar except for the extension of the maximum displacement zone. In the case of the unreinforced retaining wall, the maximum displacement occurred on the outer surface of the wall indicating that a larger part of the soil moves outward relative to the wall leading to the failure of the retaining wall. While the wall incorporated with the geocell mattresses shows maximum displacement zone is laterally extended towards the backfill. This indicates that geocells provide confinement to the soil and restrict the lateral deformation in an outward direction. Hence, it can be said that with the provision of geocell mattresses, the retaining wall is able to prevent the lateral movement of the soil mass in an outward direction. Additionally, the factor of safety significantly increases from 0.86 to 1.56 by adding geocell layers within the retaining wall system.

3.3 Effect of the Wall's Facing Angle

The influence of the facing angle on the behaviour of the geocell-reinforced retaining wall is presented in this section. The GRRW is modelled for various sloping angles 50°, 60°, 70°, and 80°, keeping a surcharge pressure of 20 kPa constant. Figure 9 illustrates the facing displacement of the wall with various sloping angles. In general, lateral displacement increases gradually with the increase in the wall's facing angle from 50 to 80°. However, the lateral displacement was found to be

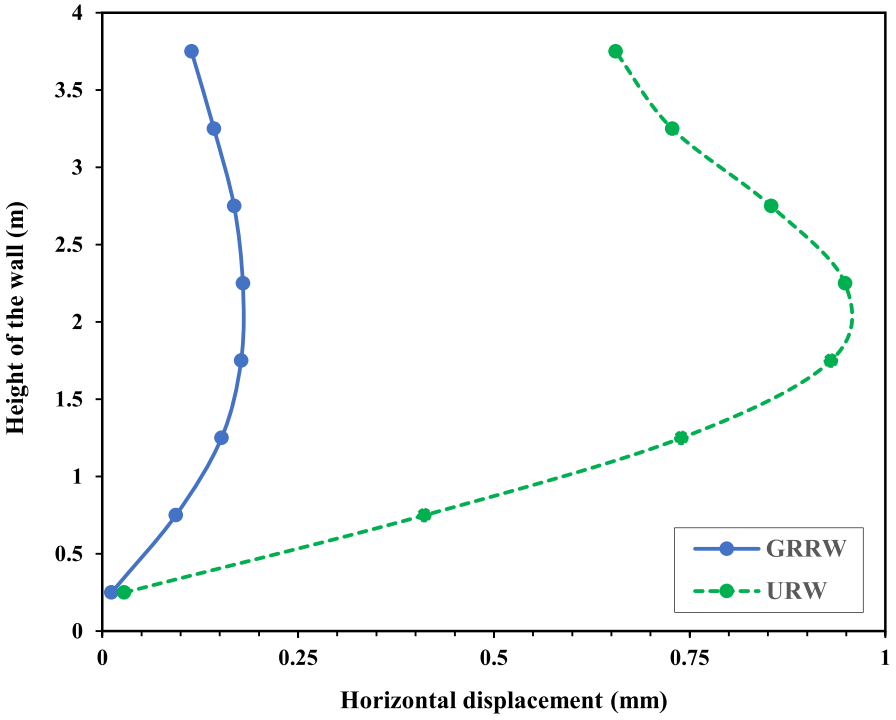
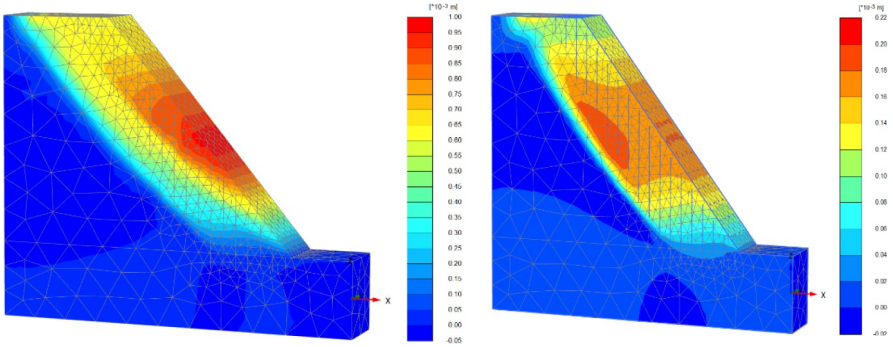


Fig. 7 Effect of provision of geocell on the horizontal displacement of retaining wall



(a) Unreinforced retaining wall (b) Geocell reinforced retaining wall

Fig. 8 Horizontal displacement contour for unreinforced and reinforced retaining wall

significantly reduced beyond the wall's facing angle of 60°. This is possibly because of the considerable reduction in the stiffness of the composite wall system (i.e., geocell-reinforced retaining wall) with an increase in the wall's facing angle from 60 to 70°, indicating that the overall stability of the wall reduced noticeably. Hence, it can be said that the geocell-reinforced retaining system is unable to provide enough

support to prevent the lateral movement of the soil mass beyond the wall's facing angle of 60°, leading to large lateral deformation in the system. It can be further observed that the displacement induced by the steep-facing wall (80°) is much greater than the gentle-facing wall (50°). For instance, the maximum displacement of the wall having a facing angle equal to 80° is 27 mm, which is reduced to 1.76 mm for the facing angle equal to 50°. Indeed, the factor of safety decreases from 1.37 to 0.78, with the increase in the wall's facing angle from 50 to 80°, respectively. The percentage reduction is found to be in the order of 75.64% with the increase in the wall's facing angle from 50 to 80°. Further, it can be noticed that moving to the steep wall's facing angle, the occurrence of maximum displacement is at 0.5625 H, 0.5625 H, 0.6875 H, and H from the bottom of the wall. This indicates that as the sloping angle increases, the development of the maximum displacement starts transitioning towards the top of the wall. It can be confirmed from the contour of horizontal displacement (U_x) of the geocell-reinforced retaining wall as shown in Fig. 10. This is because the centre of gravity of the steep-facing wall lies closer to the wall face which makes it less resistant to overturning than the gentle-facing wall. Furthermore, the contour of lateral displacement of geocell reinforcement shows almost a similar trend as that of geocell-reinforced walls. Figure 11 indicates the contour of the horizontal displacement of the geocell. The occurrence of maximum displacement shifted from mid to top with an increase in the facing angle. It can also be seen from the figure that for the gentle-facing angle, the bottom layer of the

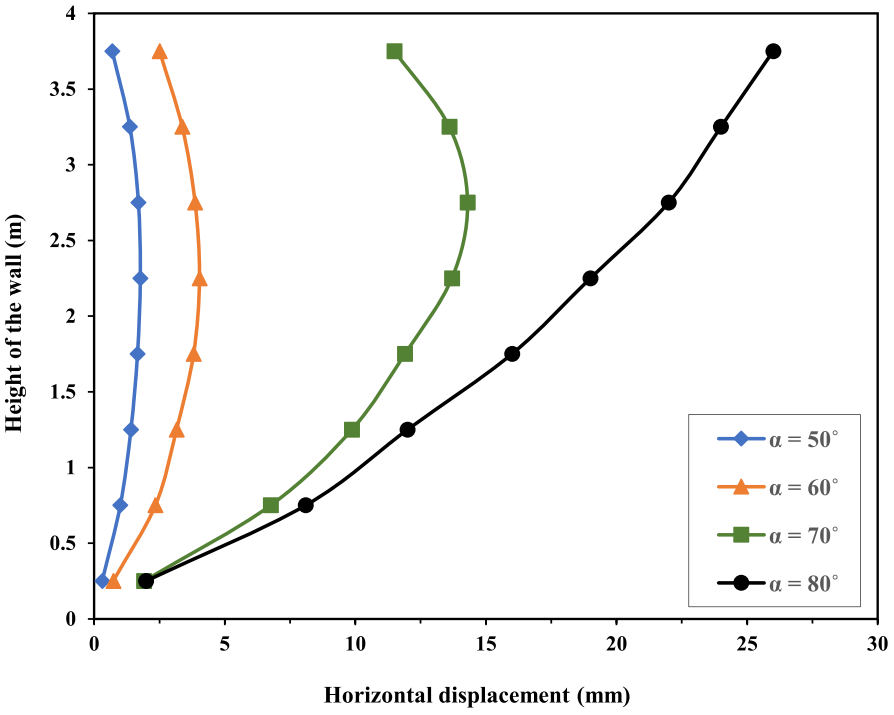


Fig. 9 Influence of sloping angle on the horizontal displacement of geocell-reinforced retaining wall

geocell mattress is able to take the load, while the contribution of the bottom layer in the case of the steep sloping angle is negligible. This is because the point of maximum displacement gets shifted towards the top of the reinforced wall. Moreover, the tensile force tends to build up in the geocells which restrain the lateral displacement. With an increase in the wall-sloping angle, the lateral movement increases, resulting in an increase in the tensile forces within the geocell mattress. This can also be verified from the contour of the axial force of the geocell. Figure 12 shows the contour of tensile force developed in the geocell reinforcement. The maximum tensile force generated in the geocell is 0.6598 kN/m for a sloping angle of 50°, and it increases to 2.572 kN/m for a sloping angle of 80°. It can be seen from the figure that the maximum tensile force is developed at the back of the wall indicating that the geocell reinforcement is able to effectively prevent the lateral movement of soil mass and hence increases the stability of the wall.

3.4 Effect of Surcharge

The influence of the surcharge on the overall behaviour of the geocell-reinforced retaining wall system has been studied under this section. The surcharge values were

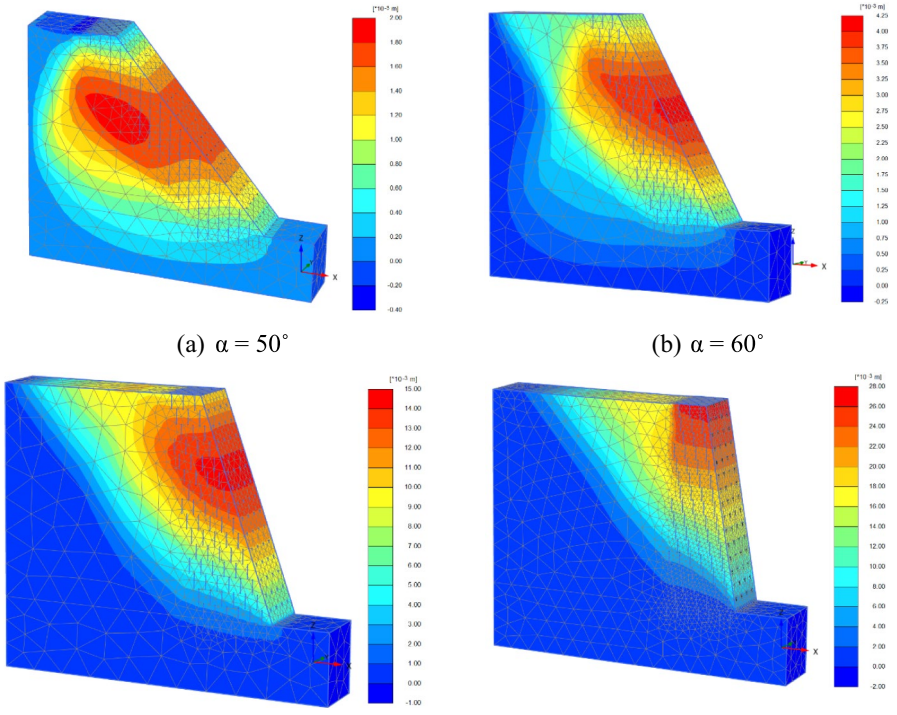


Fig. 10 Displacement contour of geocell-reinforced retaining wall for different facing angle

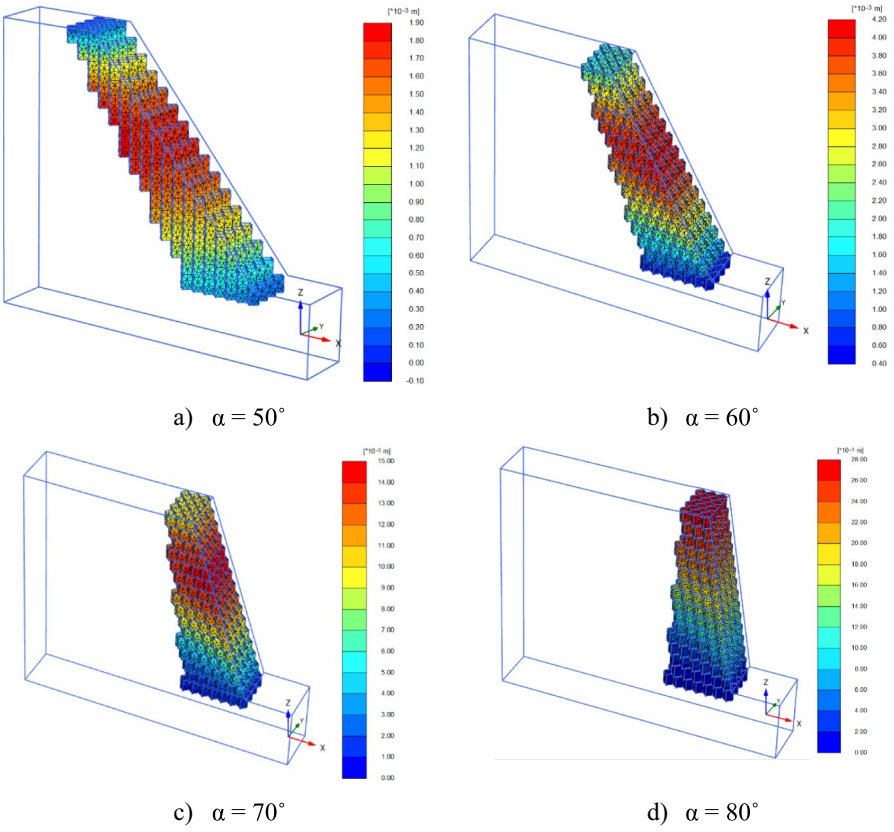
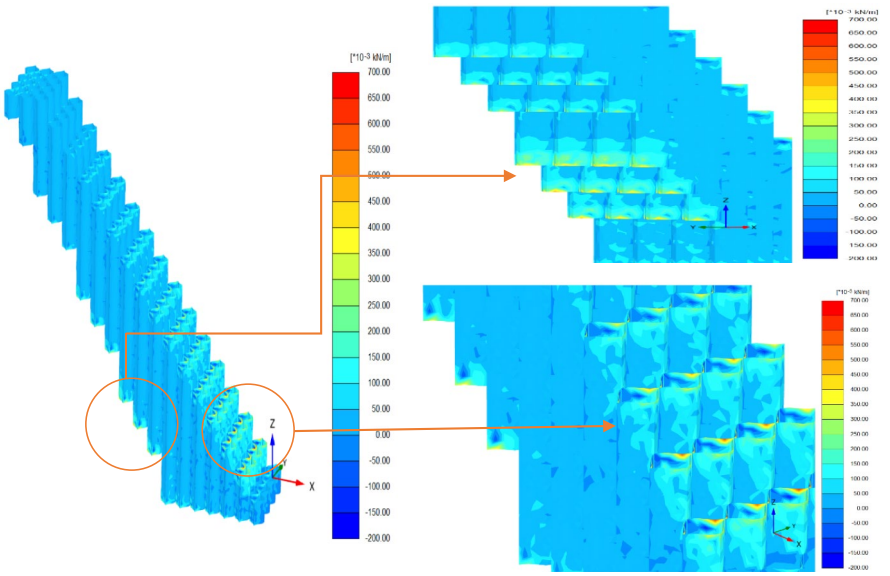
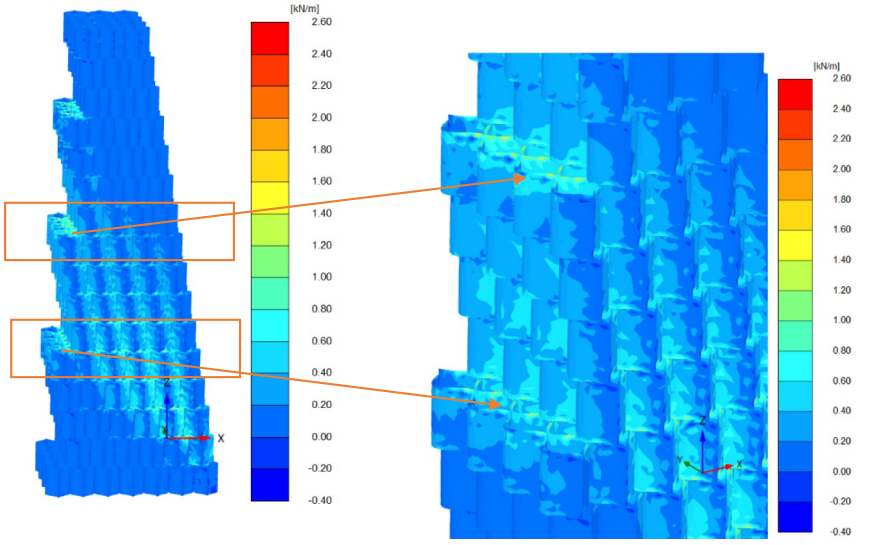


Fig. 11 Displacement contour of geocell reinforcement at various sloping angles

varied (i.e., 0 kPa, 20 kPa, 45 kPa, and 70 kPa) while keeping the wall facing angle constant at 60°. It is found that with the increase in the surcharge pressure, the factor of safety of the retaining wall system decreases considerably. By increasing the surcharge from 0 to 70 kPa, the FOS decreases from 1.56 to 0.98. This is because increased surcharge leads to stress concentration on the wall's facing, thereby decreasing the overall factor of safety. Further, it can be observed that the lateral displacement of the wall is greatly influenced by the surcharge pressure (i.e., 0 to 70 kPa) as shown in Fig. 13. For example, the facing displacement obtained for a 0 kPa surcharge is negligible (i.e., 0.084 mm) which has been increased to 24.37 mm for a surcharge pressure of 70 kPa. However, beyond the surcharge pressure of 20 kPa, a sudden rise in lateral displacement was observed. For example, the facing displacement obtained for 20 kPa surcharge is found to be nearly 3.9 mm which has been increased to 17.4 mm for the surcharge pressure of 45 kPa. The percentage increase in the lateral displacement was found to be in the order of 346% with an increase in the surcharge pressure from 20 to 45 kPa. This is possibly due to the vertical deformation of the top layer of geocell reinforcement under concentrated increased



a) Maximum value = 0.6598 kN/m ($\boldsymbol{\alpha = 50^{\circ}}$)



b) Maximum value = 2.572 kN/m ($\boldsymbol{\alpha = 80^{\circ}}$)

Fig. 12 Contour of axial displacement of geocell reinforcement for different sloping angles

surcharge load. As a result, the lateral resistance offered by the upper part of geocell reinforcement reduces significantly leading to a considerable deformation in the composite system. This can be more clearly observed through displacement contours as presented in Fig. 14. The contour of the reinforced wall shows that with an

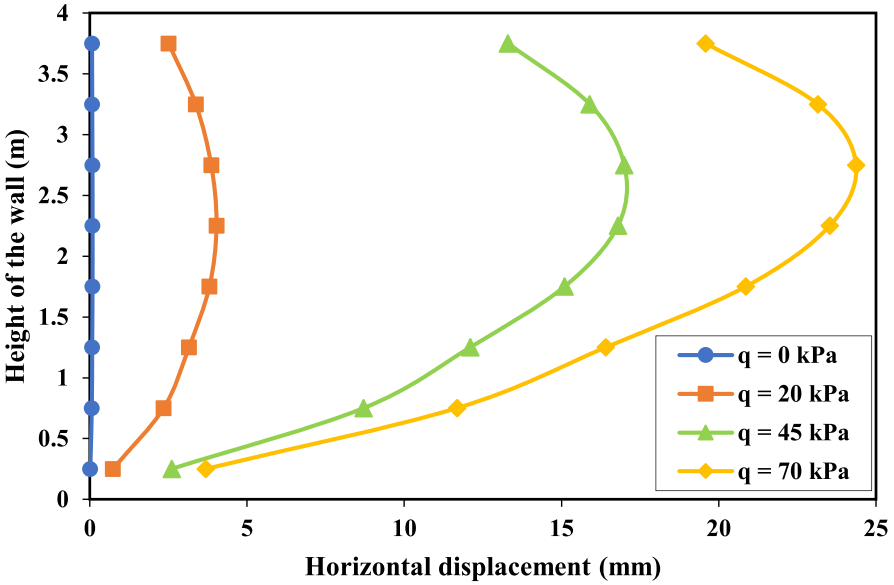
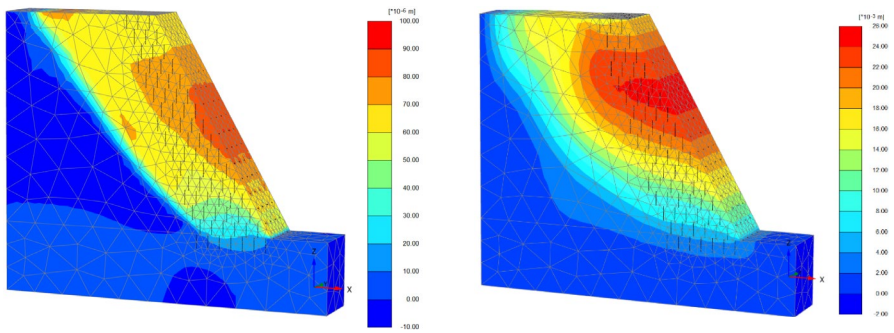


Fig. 13 Effect of surcharge on the horizontal displacement of the geocell-reinforced retaining wall

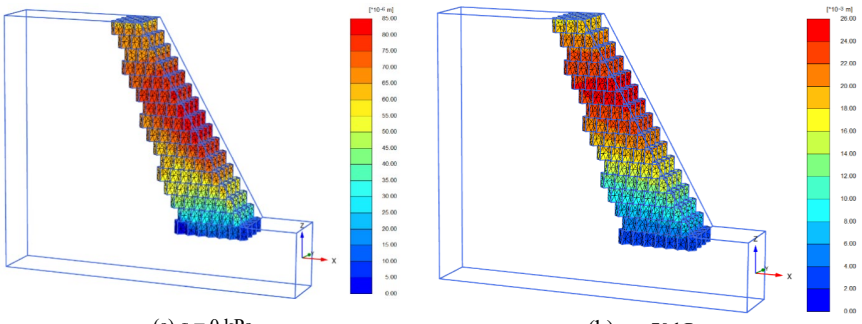
increase in the surcharge load, the influence zone of displacement shifted upwards as well as extended laterally. This can also be depicted from the contour that for higher surcharge pressure, the wall is more prone to deep-seated failure. Hence, it can be said that at a slope angle of 60°, the retaining wall of a given geometry can sustain a surcharge pressure of up to 45 kPa beyond which the wall is on the verge of failure.

Further, the displacement contour of the geocell mattress for the surcharge pressure of 0 and 70 kPa is presented in Fig. 15. From the figure, it can be seen that the displacement pattern in geocell reinforcement is found to be similar for both cases.



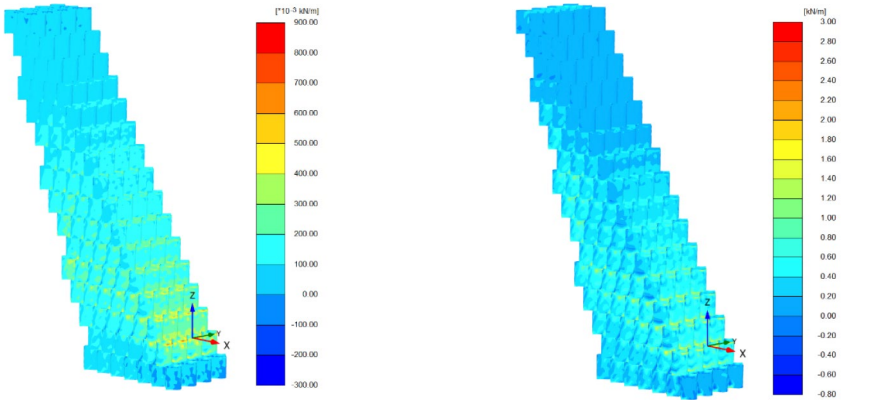
(a) q = 0 kPa (b) q = 70 kPa

Fig. 14 Contour of lateral displacement for the reinforced retaining wall at different surcharge pressures



(a) q = 0 kPa (b) q = 70 kPa

Fig. 15 Contour of the lateral displacement for the geocell mattress at different surcharge pressures



a) Max. value = 0.8696 kN/m (q = 0 kPa) b) Max. value = 2.812 kN/m (q = 70 kPa)

Fig. 16 Axial force developed in the geocell reinforcement for different surcharge pressure

However, the magnitude of displacement is found to increase with the increase in the surcharge pressure. The tensile force developed in the geocell reinforcement is also reported in Fig. 16. It is of interest to note that in all the cases, the tensile forces are found to be more in the opposite face of the wall. Further, the tensile forces were found to be maximum at a surcharge pressure of 70 kPa i.e., 2.812 kN/m, while for no surcharge, it attains a value of 0.8696 kN/m. It clearly indicates that the development of the increased tensile force takes place in the geocell reinforcement with an increase in surcharge pressure. Hence, due to its semi-rigid behaviour, it can sustain the upcoming lateral load until the large deformation, thereby preventing the sudden failure in the composite retaining system.

3.5 Effect of the Axial Stiffness of the Geocell

The stiffness of the geocell is a crucial factor for determining the stability and failure mechanism of the geocell-reinforced wall. This section deals with the influence of the axial stiffness of the geocell on the deformation behaviour of GRRW. To investigate the impact, the axial stiffness of the geocell mattress is varied (i.e., 150 kN/m, 250 kN/m, 350 kN/m, 492 kN/m, 750 kN/m, 1000 kN/m, 1500 kN/m, 1800 kN/m, 2000 kN/m, and 2460 kN/m) in the retaining wall system. The wall-facing angle and surcharge of the wall are kept constant at 60° and 20 kPa, respectively. Figure 17 shows the facing displacement profile of the wall with varying stiffness of the geocell mattress. It is found that with the increase in stiffness of the geocell, the lateral displacement of the wall decreases. However, beyond the axial stiffness of 1800 kN/m, the decrement in the horizontal displacement becomes nominal. This can be explained by the fact that due to an increase in the stiffness of the geocell mattress, the overall rigidity of the reinforced wall increases which leads to the distribution of the load over a wider area and prevents the lateral deformation in the wall significantly. However, beyond 1800 kN/m the rigidity of the wall remains the same,

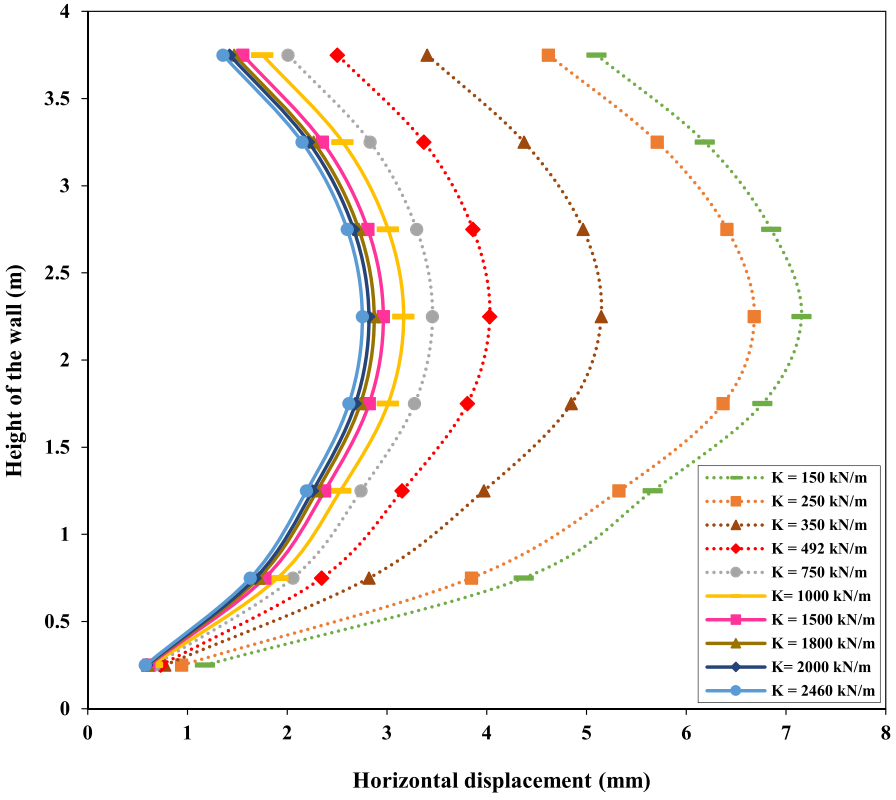
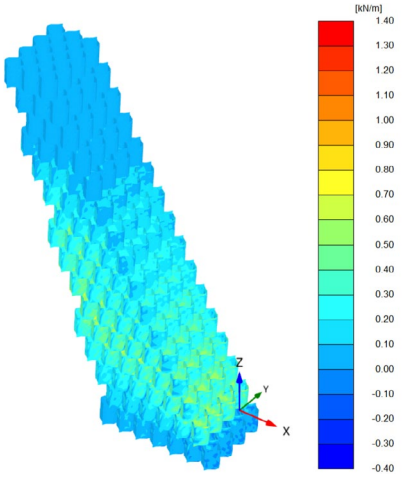


Fig. 17 Influence of axial stiffness on the horizontal displacement of the wall

because of which further decrement in the displacement is minimal. Further, the tensile force gets developed in the geocell mattress, which prevents the lateral displacement occurring in the wall. From the contours of tensile force, it is visible that the maximum tensile force developed in the geocell is 1.798 kN/m and 1.315 kN/ for stiffness values 2460 kN/m and 150 kN/m, respectively (Fig. 18). That means the tensile force is higher for higher stiffness of geocell mattress. This is possibly because of the reason that with the increase in the stiffness of the geocell mattresses, the reinforcement behaves as a stiffer cushion due to which higher tensile force developed in the geocell mattress. Hence, it can be deduced that with an increase in the stiffness of the geocell mattress, the lateral displacement of the wall decreases due to an increase in the rigidity of the mattresses. However, beyond 1800 kN/m, the rigidity remains the same and thus provides minimal decrement in the displacement.

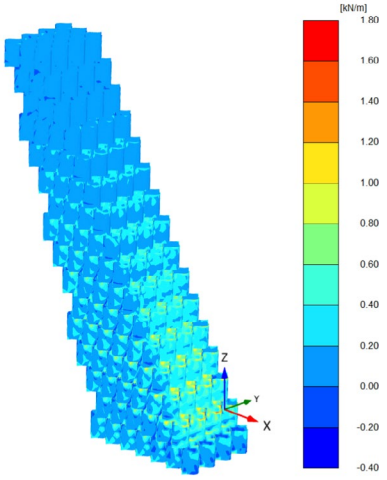
3.6 Effect of the Height of the Geocell Mattress

The height of the geocell mattress is one of the parameters which could affect the performance of the geocell-reinforced retaining wall system. The considered height of geocell mattresses are 125 mm, 250 mm, and 500 mm keeping a constant sloping angle of 60°. The number of layers of reinforcement is changed according to the height of the geocell mattress. For 125 mm height, 32 layers of geocell mattresses are required. Similarly, 16 layers for 250 mm and 8 layers for 500 mm are inserted into the wall. Figure 19 represents the variation of horizontal displacement of the wall with different heights of geocell mattresses. It is



Max. Value = 1.315 kN/m

(a) EA= 150 kN/m



Max. Value = 1.798 kN/m

(b) EA= 2460 kN/m

Fig. 18 Contour of axial force developed in the geocell at different axial stiffness of the geocell

found that with the increase in the height of the geocell mattress, the performance of the GRRW gets improved, that is, its lateral displacement decreases. As the height of the geocell mattress increases from 125 to 250 mm, the displacement of the wall facing decreases significantly. Further, when the height of the geocell mattress increased from 250 to 500 mm, the decrement in the facing displacement is marginal. This is possibly because, for the geocell height of 125 mm, a large number of geocell mattresses have to be provided to attain the full height of the retaining wall. More layers of geocell mattresses mean a greater number of joints which results in greater facing displacement to the wall. Further, when the height of the geocell mattress increases to 500 mm, the wall exhibits a marginal effect suggesting that the rigidity of the geocell mattress decreases. This decrease in rigidity results in a comparable level of performance. This can be affirmed by the displacement contour of the geocell, which has been presented in Fig. 20. Therefore, it can be concluded that increasing the height of the geocell mattress leads to a decrease in facing displacement. If the height of the geocell is increased from 125 to 250 mm, the decrement is significant. Further, if it increased to 500 mm, the decrement in displacement is marginal.

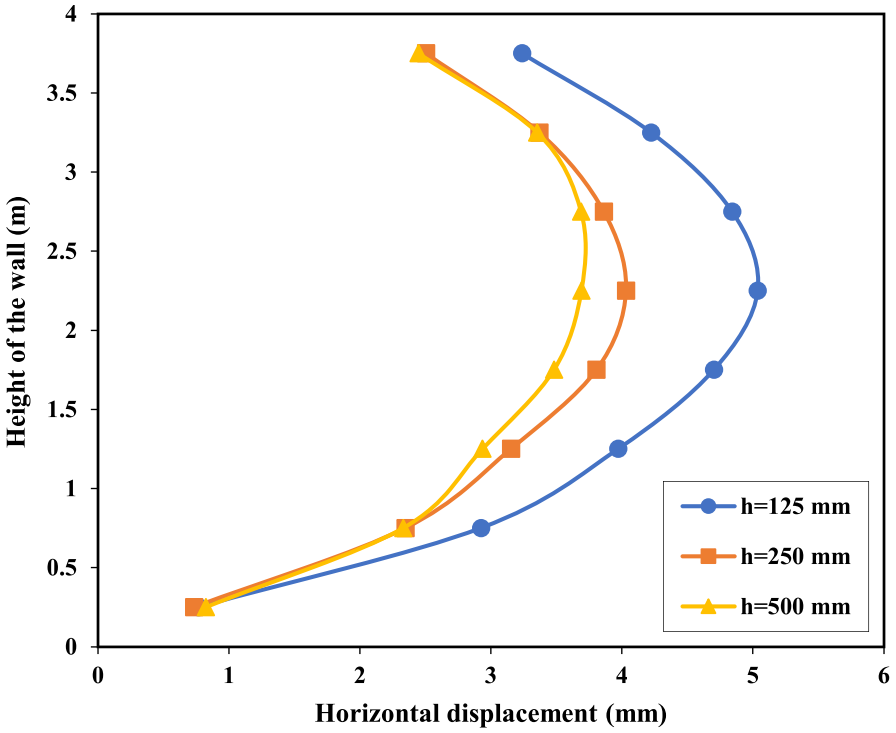


Fig. 19 Effect on the horizontal displacement of the wall for different heights of the geocell

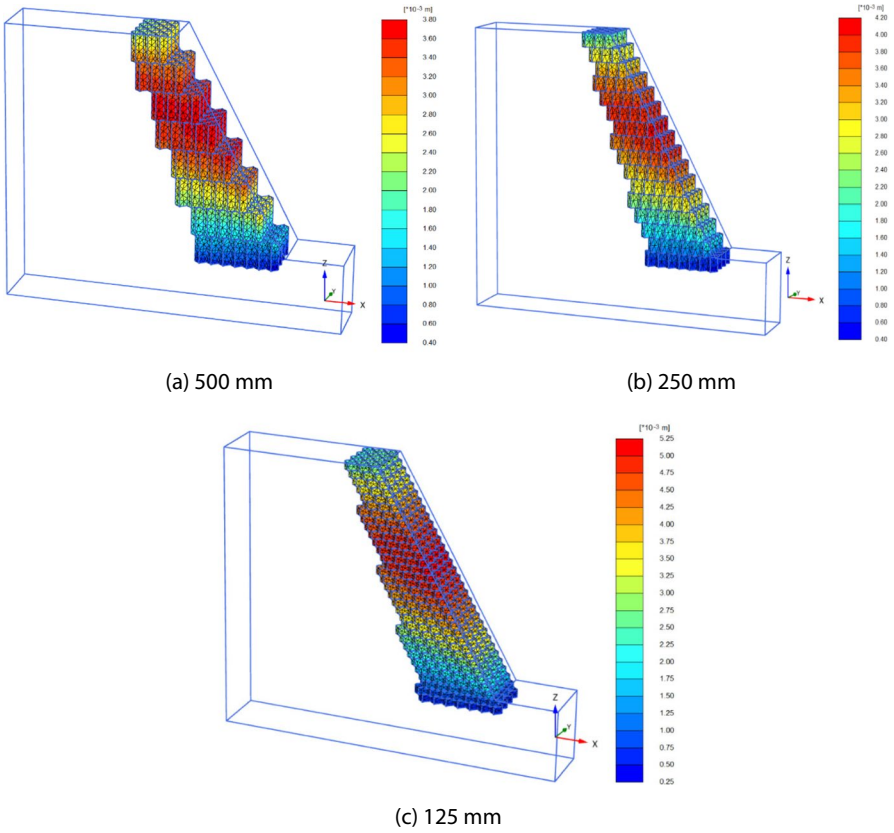


Fig. 20 Contour of the horizontal displacement for various heights of the geocell

3.7 Effect of the Friction Angle of the Soil

The stability of the geocell-reinforced retaining wall is highly influenced by the shear strength parameter of soil used as a backfill or infill soil. In view of this, the influence of friction angle (ϕ) of soil has been investigated on the behaviour of geocell-reinforced retaining wall systems. The value of the friction angle is varied (i.e., 35°, 40°, and 45°). Correspondingly, the value of the dilation angle (ψ) is obtained as $\psi = \phi - 30°$. Figure 21 shows the displacement profile of the wall with varying friction angles of soil. It is found that the horizontal displacement of the retaining wall decreases with an increase in friction angle. Here, for $\phi = 35°$, the maximum displacement in the wall is 4.03 mm and it decreases to 1.05 mm for $\phi = 45°$. This can be elucidated by the fact that with an increase in the friction angle, the shear strength of soil increases. As a result, the interaction between the soil and geocell interface improves. This improved interaction leads to a higher utilisation of shear strength at the interface and reduces the lateral displacement of the wall. This is why the factor of safety also increased by 1.4 times by changing the ϕ value from 35 to

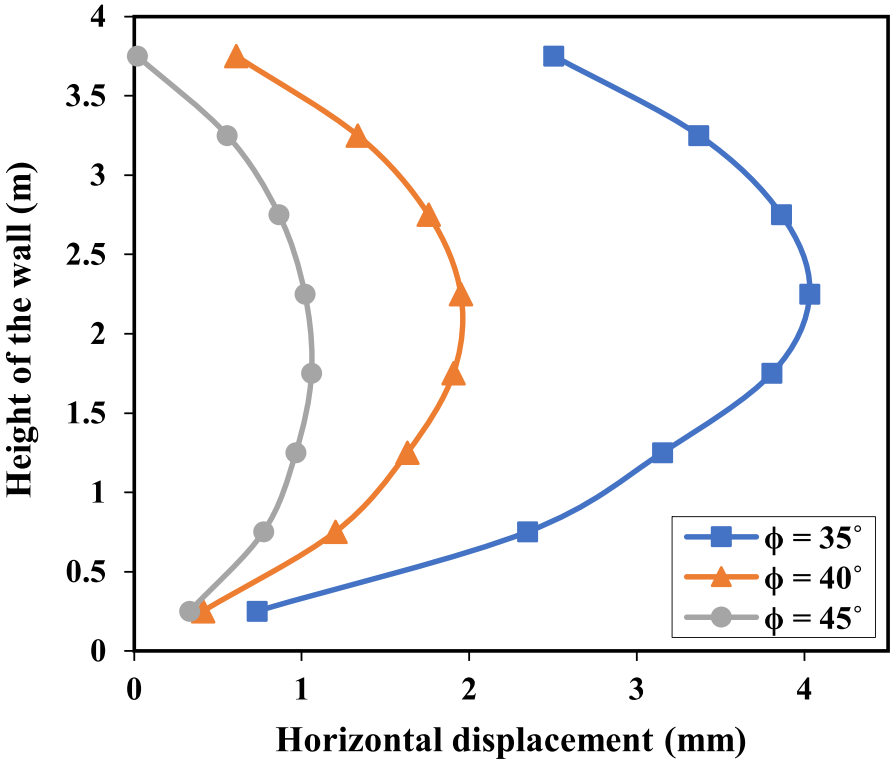


Fig. 21 Effect on the horizontal displacement of the wall for different friction angles of soil

45°. Hence, it can be stated that better performance of geocell-reinforced retaining wall systems can be achieved with a higher friction angle of soil mass.

3.8 Effect of the Dilation Angle of the Soil

Dilatancy is a part of the soil frictional strength which will result in volume change during shear. It is characterised by dilation angle (ψ). The analysis used an immutable friction angle of 40° while the dilation angle is changed from 5 to 40°. The result shows that the lateral deformation decreases with an increase in dilation angle (Fig. 22). For instance, the maximum displacement occurring in the wall is 2.15 mm for $\psi = 5°$ and it decreases drastically to 1.13 mm for $\psi = 40°$. It could be explained by the reason that when the shear stress is gradually increased, the soil particles rearrange themselves in such a way that they can resist the force to the maximum. That means when subjected to high levels of stress, a larger volume of soil participates in resisting the force. Due to this, the mobilisation of shear strength at the soil–geocell interface increases significantly. As a result, the facing displacement of the reinforced wall system decreases with the increase in the dilation angle of soil mass.

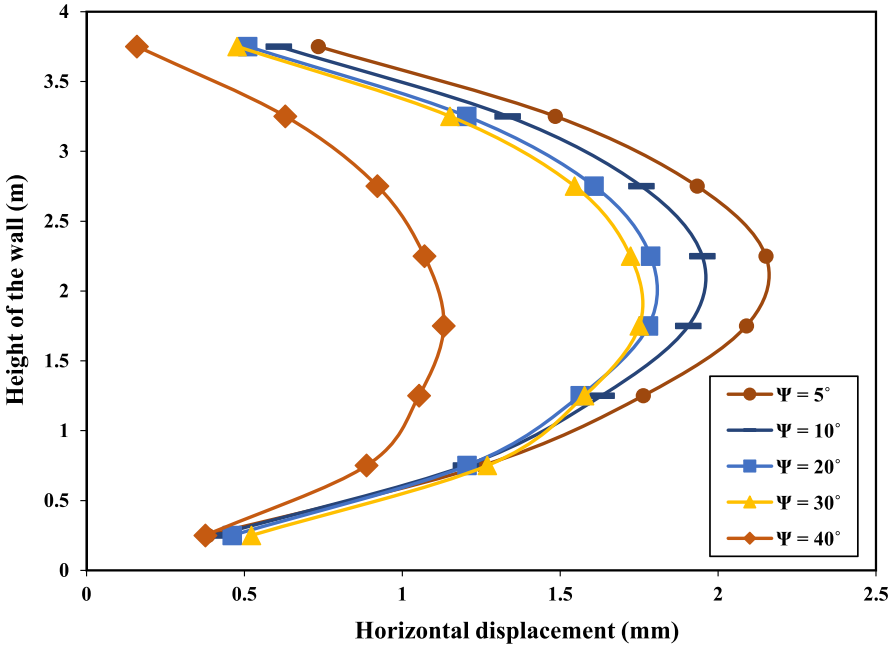


Fig. 22 Effect on the horizontal displacement of the wall for different dilation angles of soil

4 Conclusion

This study presents a numerical analysis on geocell-reinforced retaining walls using the finite element method PLAXIS^{3D}. The numerical models are validated with the experimental results, thereafter extensive studies have been carried out. The major distinction of this study is the modelling of the geocell by considering the actual expanded honeycomb shape of the geocell. The behaviour of retaining walls by incorporating the multiple layers of geocell mattresses has been studied. Furthermore, the influences of sloping angle, surcharge pressure, stiffness and height of geocell mattress, friction, and dilation angle of the soil on the behaviour of composite retaining wall system have also been reported. Based on the results, the following conclusions are drawn:

(1) The honeycomb shape of the geocell is successfully simulated in PLAXIS^{3D}. Besides, the proposed model is found to be efficient in simulating the experimental results indicating that the present model can be considered to investigate the overall behaviour of geocell reinforcement retaining wall system.
(2) The inclusion of the layers of the geocell mattresses to unreinforced retaining walls improves its performance significantly in terms of lateral deformation and factor of safety. The lateral displacement of the wall decreases by 81% with the incorporation of geocell mattresses into the unreinforced retaining wall. Moreover, the factor of safety of unreinforced retaining wall is 0.86 which increases to 1.56 for geocell-reinforced retaining wall system.

(3) The facing displacement of the wall increases with an increase in the facing angle of the reinforced wall system. That is the lateral displacement is lower for the gentle slope facing wall ($\alpha = 50°$) than steep facing wall ($\alpha = 80°$). Further, proceeding to the steeper facing wall, the occurrence of the maximum displacement moves from mid to the top of the wall. Besides, the factor of safety of the reinforced wall system decreased by nearly 1.75 times when the facing angle was changed from 50 to 80°.
(4) The surcharge pressure applied on the backfill also has a significant effect on the geocell-reinforced wall system. The lateral displacement of the wall increases with an increase in the surcharge pressure. Here, the displacement observed when no surcharge is applied is about 0.084 mm, but it significantly increases to 24.37 mm when a surcharge of 70 kPa is added to the backfill of the wall.
(5) As the stiffness of the geocell mattress increases, the lateral displacement of the wall decreases. This relationship holds true until a stiffness of 1800 kN/m. Beyond this, the decrement in lateral displacement becomes minimal implying that the rigidity of the geocell mattresses remains the same thereafter.
(6) Increasing the height of the geocell mattress enhances the performance of the geocell-reinforced retaining wall. As the height of the geocell mattress increases from 125 to 250 mm, a noticeable decrease in lateral displacement is observed. However, when the height of the geocell mattress is further increased to 500 mm, the impact on the wall's behaviour is minimal.
(7) The increase in the friction angle of the soil improves the performance of the geocell-reinforced wall system. For $\phi = 35°$, the wall exhibits a maximum displacement of 4.03 mm, whereas this displacement decreases to 1.05 mm when the ϕ is increased to 40°. Furthermore, by increasing the ϕ value from 35 to 45°, the factor of safety of the composite wall system experiences a significant increase of 1.4 times.
(8) The geocell-reinforced wall system is notably influenced by the dilation angle of the soil. With an increase in the dilation angle, the facing displacement of the wall decreases. Herein, the wall experiences a substantial decrease in the maximum displacement from 2.15 mm at $\psi = 5°$ to 1.13 mm at $\psi = 40°$.

The outcome of the present study highlighted the efficacy of geocell reinforcement in increasing the stability of the retaining wall system. The results could be used to provide a general approach for the design and construction of a geocell-reinforced retaining wall system. Besides, this study will help researchers to understand the insight behaviour of reinforced retaining walls to carry out their further research in this field. However, to get a more realistic outcome, a field study needs to be performed by considering different aspects of the geocell-reinforced retaining wall system.

Acknowledgements The authors are thankful to the anonymous reviewers for their critical comments and suggestions which have been very useful in improving the quality of the manuscript.

Author Contributions All three authors have contributed in the preparation of the entire manuscript. The submitted paper was meticulously checked and approved by the authors.

Data Availability The datasets are available from the corresponding author on reasonable request.

Declarations

Ethics Approval and Consent to Participate Not applicable.

Consent for Publication Not applicable.

Competing interests The authors declare no competing interests.

References

Arvin, M.R., Sooreshjani, H.M., Khademhosseini, A.: Behaviour of geocell-reinforced strip footings on slopes. Geomech. Geoeng. (2022). https://doi.org/10.1080/17486025.2021.1912404

Bathurst, R.J., Huang, B., Hatami, K.: Numerical modeling of geosynthetic reinforced soil walls. In: Linear and Non-Linear Numerical Analysis of Foundations (2001). https://doi.org/10.1201/9781482265958-10

Benjamim, C.V.S., Bueno, B.S., Zornberg, J.G.: Field monitoring evaluation of geotextile-reinforced soil-retaining walls. Geosynth. Int. (2007). https://doi.org/10.1680/gein.2007.14.2.100

Bush, D.I., Jenner, C.G., Bassett, R.H.: The design and construction of geocell foundation mattresses supporting embankments over soft grounds. Geotext. Geomembr. (1990). https://doi.org/10.1016/0266-1144(90)90006-X

Chen, R.H., Chiu, Y.M.: Model tests of geocell retaining structures. Geotext. Geomembr. (2008). https://doi.org/10.1016/j.geotexmem.2007.03.001

Chen, R.H., Wu, C.P., Huang, F.C., Shen, C.W.: Numerical analysis of geocell-reinforced retaining structures. Geotext. Geomembr. (2013). https://doi.org/10.1016/j.geotexmem.2013.07.003

Cheng, Y.M., Lansivaara, T., Wei, W.B.: Two-dimensional slope stability analysis by limit equilibrium and strength reduction methods. Comput. Geotech. (2007). https://doi.org/10.1016/j.compgeo.2006.10.011

Choudhary, A.K., Pandit, B., Babu, G.L.S.: Uplift capacity of horizontal anchor plate in geocell reinforced sand. Geotext. Geomembr. (2019). https://doi.org/10.1016/j.geotexmem.2018.12.009

Dash, S.K., Choudhary.: A.K.: Geocell reinforcement for performance improvement of vertical plate anchors in sand. Geotext. Geomembr. (2018). https://doi.org/10.1016/j.geotexmem.2017.11.008

Dash, S.K., Krishnaswamy, N.R., Rajagopal, K.: Bearing capacity of strip footings supported on. Geotext. Geomembr. **19**(4), 235–256 (2001)

Dash, S.K., Sireesh, S., Sitharam, T.G.: Model studies on circular footing supported on geocell reinforced sand underlain by soft clay. Geotext. Geomembr. (2003). https://doi.org/10.1016/S0266-1144(03)00017-7

Griffiths, D.V., Marquez, R.M.: Three-dimensional slope stability analysis by elasto- plastic finite elements. Geotechnique. (2007). https://doi.org/10.1680/geot.2007.57.6.537

Halder, K., Chakraborty, D.: Influence of soil spatial variability on the response of strip footing on geocell-reinforced slope. Comput. Geotech. (2020). https://doi.org/10.1016/j.compgeo.2020.103533

Hegde, A., Sitharam, T.G.: 3-Dimensional numerical modelling of geocell reinforced sand beds. Geotext. Geomembr. (2014). https://doi.org/10.1016/j.geotexmem.2014.11.009

Hegde, A., Sitharam, T.G.: Experiment and 3D-numerical studies on soft clay bed reinforced with different types of cellular confinement systems. Transp. Geotech. (2017). https://doi.org/10.1016/j.trgeo.2017.01.001

Hegde, A.M., Sitharam, T.G.: Experimental and numerical studies on protection of buried pipelines and underground utilities using geocells. Geotext. Geomembr. (2015). https://doi.org/10.1016/j.geotexmem.2015.04.010

Krishnaswamy, N.R., Rajagopal, K., Latha, G.M.: Model studies on geocell supported embankments constructed over a soft clay foundation. Geotech. Test. J. (2000). https://doi.org/10.1520/gtj11122j

Latha, G.M., Dash, S.K., Rajagopal, K.: Numerical simulation of the behavior of geocell reinforced sand in foundations. Int. J. Geomech. (2009). https://doi.org/10.1061/(asce)1532-3641(2009)9:4(143)

Latha, G.M., Rajagopal, K.: Parametric finite element analyses of geocell-supported embankments. Can. Geotech. J. **44**(8), 917–927 (2007)

Latha, G.M., Somwanshi, A.: Effect of reinforcement form on the bearing capacity of square footings on sand. Geotext. Geomembr. (2009). https://doi.org/10.1016/j.geotexmem.2009.03.005

Mehdipour, I., Ghazavi, M., Moayed, R.Z.: Numerical study on stability analysis of geocell reinforced slopes by considering the bending effect. Geotext. Geomembr. (2013). https://doi.org/10.1016/j.geotexmem.2013.01.001

Rowe, R.K., Skinner, G.D.: Numerical analysis of geosynthetic reinforced retaining wall constructed on a layered soil foundation. Geotext. Geomembr. (2001). https://doi.org/10.1016/S0266-1144(01)00014-0

Song, F., Liu, H., Chai, H., Chen, J.: Stability analysis of geocell-reinforced retaining walls. Geosynth. Int. (2017). https://doi.org/10.1680/jgein.17.00013

Song, F., Liu, H., Ma, L., Hu, H.: Numerical analysis of geocell-reinforced retaining wall failure modes. Geotext. Geomembr. (2018). https://doi.org/10.1016/j.geotexmem.2018.01.004

Zornberg, J.G., Sitar, N., Mitchell, J.K.: Closure to performance of geosynthetic reinforced slopes at failure. J. Geotech. Geoenviron. Eng. (1998). https://doi.org/10.1061/(asce)1090-0241(2000)126:3(285)

Publisher's Note Springer Nature remains neutral with regard to jurisdictional claims in published maps and institutional affiliations.

Springer Nature or its licensor (e.g. a society or other partner) holds exclusive rights to this article under a publishing agreement with the author(s) or other rightsholder(s); author self-archiving of the accepted manuscript version of this article is solely governed by the terms of such publishing agreement and applicable law.